catalysts

MDPI

Article

PtAu Nanoparticles Supported by Reduced Graphene Oxide as a Highly Active Catalyst for Hydrogen Evolution

Lazar Rakočević [1], Ivana Stojković Simatović [2], Aleksandar Maksić [1], Vladimir Rajić [1], Svetlana Štrbac [3] and Irina Srejić [1,*]

[1] INS Vinca, Department of Atomic Physics, University of Belgrade, Mike Petrovića Alasa 12–14, 11351 Belgrade, Serbia; lazar.rakocevic@vinca.rs (L.R.); maxa@vinca.rs (A.M.); vladimir.rajic@vinca.rs (V.R.)
[2] Faculty of Physical Chemistry, University of Belgrade, Studentski trg 12–16, 11158 Beograd, Serbia; ivana@ffh.bg.ac.rs
[3] Department of Electrochemistry, Institute of Chemistry, Technology and Metallurgy, University of Belgrade, Njegoševa 12, 11000 Belgrade, Serbia; sstrbac@tmf.bg.ac.rs
* Correspondence: irina@vinca.rs

Abstract: PtAu nanoparticles spontaneously deposited on graphene support, PtAu/rGO, have shown remarkably high catalytic activity for hydrogen evolution reaction (HER) in sulfuric acid solution. SEM images of the PtAu/rGO electrode surface showed that Pt nanoparticles that are non-uniform in size occupy both the edges of previously deposited uniform Au nanoparticles and the edges of graphene support. XPS analysis showed that the atomic percentages of Au and Pt in PtAu/rGO were 0.6% and 0.3%, respectively. The atomic percentage of Au alone on previously prepared Au/rGO was 0.7%. Outstanding HER activity was achieved for the PtAu/rGO electrode, showing the initial potential close to the equilibrium potential for HER and a low Tafel slope of −38 mV/dec. This was confirmed by electrochemical impedance spectroscopy. The chronoamperometric measurement performed for 40 min for hydrogen evolution at a constant potential indicated good stability and durability of the PtAu/rGO electrode.

Keywords: platinum; gold; PtAu nanoparticles; graphene; SEM; XPS; hydrogen evolution

check for updates

Citation: Rakočević, L.; Simatović, I.S.; Maksić, A.; Rajić, V.; Štrbac, S.; Srejić, I. PtAu Nanoparticles Supported by Reduced Graphene Oxide as a Highly Active Catalyst for Hydrogen Evolution. *Catalysts* **2022**, *12*, 43. https://doi.org/10.3390/catal12010043

Academic Editors: Vincenzo Baglio and Shuhui Sun

Received: 16 November 2021
Accepted: 28 December 2021
Published: 31 December 2021

Publisher's Note: MDPI stays neutral with regard to jurisdictional claims in published maps and institutional affiliations.

Copyright: © 2021 by the authors. Licensee MDPI, Basel, Switzerland. This article is an open access article distributed under the terms and conditions of the Creative Commons Attribution (CC BY) license (https://creativecommons.org/licenses/by/4.0/).

1. Introduction

Hydrogen evolution reaction (HER) is one of the most extensively studied reactions in electrocatalysis due to its general importance, from both a fundamental and practical point of view. The world needs an alternative to fossil fuels, economically and from an environmental aspect. Since hydrogen is a simple and "clean" energy carrier, it is an excellent fuel produced by water splitting through the hydrogen evolution reaction [1–3]. The efficient and cost-effective hydrogen production process requires a suitable catalyst for HER. A catalyst should be cheap with great activity, stability, and durability. It is well known that platinum group metals are the best electrocatalysts, with Pt on the top, for hydrogen evolution reaction, but very expensive and scarce to be the electrode materials. Therefore, the aim is to find a more economical catalyst with the best possible performances. The studies are focused on obtaining catalysts either with a low content of precious [4,5] or non-precious metals [6] supported by carbon-based materials.

Recently, single-atom catalysts made a breakthrough in the catalysis of the hydrogen evolution reaction [7,8]. There are many reports in the literature on precious [9–11] and non-precious metal single-atom catalysts [12–14], from the synthesis to their usage as catalysts for HER and other reactions of importance for fuel cells and electrolyzers. The density-functional theory (DFT) calculations and machine-learning techniques are valuable tools for the theory-guided design of advanced suitable catalysts for reactions in different power devices, including HER [15].

Carbon-based materials have attracted attention as excellent supports for various metallic catalysts [16]. They have many advantages, including their availability, low cost, and stability in acid and alkaline solutions. Most importantly, for hydrogen evolution electrocatalysis, these supports provide a large surface area, high electronic conductivity, and suitability for the deposition and growth of smaller catalytic particles, including mono- and multi-metallic nanoparticles. Besides, a synergetic effect between the carbon support and the catalyst leads to the better catalytic activity of the electrode.

Graphene is one of the carbon-based materials that has become very interesting for researchers after the first report on the syntheses of thin graphene sheets and their remarkable electronic properties [17]. Besides, the two-dimensional structure of graphene provides extraordinary electrical, mechanical, and optical properties, excellent thermal conductivity, and electron mobility. Hence, graphene, as well as its derivatives graphene oxide (GO) and reduced graphene oxide (rGO), have found application as catalyst supports for HER and many other reactions [18–20].

Previously, we showed that PdAu nanoparticles (NPs) supported on rGO were excellent catalysts for HER, showing low Tafel slope, low onset potential, and high current density under the same conditions [21]. Additionally, there are reports in the literature on electrocatalysts consisting of various PtAu nanoparticles supported on different carbon-based materials that have shown good performances for HER in the same 0.5 M H_2SO_4 solution. Among reduced graphene oxide-supported bimetallic AuPt catalysts, core–shell Au@Pt nanoparticles synthesized using various methods have exceptionally high HER activity. Among them, Au@Pt NPs/rGO, fabricated by a simple one-pot aqueous approach [22], Au-monolayer Pt/rGO via layer-by-layer growth of Pt monolayers on Au NPs using the electrochemical methods [23], AuPt@Pt nanocrystals/rGO produced by the addition of Au and Pt depositing salts to the rGO suspension [24], and AuPt alloy nanodendrites/rGO [25] synthesized by a one-pot reduction approach using ionic liquid.

The spontaneous deposition at the open circuit potential (OCP) of precious metals from aqueous solutions containing depositing metal salts is a very simple and easy method that is used for the preparation of electrodes with a low amount of precious metal(s). We demonstrated in our previous work [21] that a successive spontaneous deposition of Au, and Pd on rGO support produced a PdAu/rGO catalyst consisting of a small amount of PdAu nanoparticles, which has shown exceptionally high HER activity. Based on that, we examined a similar PtAu/rGO system, expecting even better HER catalytic activity.

In this paper, the preparation of Au/rGO and PtAu/rGO working electrodes involved subsequent spontaneous deposition of Au and Pt on graphene support. The techniques used for the electrodes surface characterization were field emission scanning electron microscope with energy dispersive X-ray spectrometer (FESEM/EDS) and X-ray photoelectron spectroscopy (XPS). The electrodes were characterized electrochemically by cyclic voltammetry (CV) in a 0.5 M H_2SO_4 solution. HER activity of obtained catalysts was examined by linear sweep voltammetry (LSV) and electrochemical impedance spectroscopy (EIS). The stability of the most active PtAu/rGO electrode was tested by chronoamperometry (CA). The electrodes surface was characterized using field emission scanning electron microscope with energy dispersive X-ray spectrometer (FESEM/EDS) and X-ray photoelectron spectroscopy (XPS). The electrochemical characterization in a 0.5 M H_2SO_4 solution was performed by cyclic voltammetry (CV). HER activity of obtained catalysts was examined by linear sweep voltammetry (LSV) and electrochemical impedance spectroscopy (EIS). The stability of the most active PtAu/rGO electrode was tested by chronoamperometry (CA).

2. Results and Discussion

2.1. Characterization of Au/rGO and PtAu/rGO

The Au/rGO and PtAu/rGO electrodes were prepared for surface characterization by SEM and XPS techniques as follows: firstly, the 30 μL of 3 g/L rGO ethanol suspension was spread on the GC disc (7 mm diameter) and dried at room temperature. After that, the prepared rGO/GC substrate was immersed at the open circuit potential in a gold depositing

solution for 10 min to prepare the Au/rGO electrode, and subsequently into platinum depositing solution for 30 min to prepare the PtAu/rGO electrode. The prepared electrodes were then dried at room temperature before being used for surface characterization. For the electrochemical characterization, the preparation of the electrodes involved the same procedure, except that 15 µL of graphene suspension was spread over a GC disc (5 mm diameter) mounted into a Teflon holder.

2.1.1. SEM/EDS Characterization

SEM results in Figure 1 show the morphology of Au/rGO and PtAu/rGO electrodes and the lateral size distribution of the corresponding individual Au and PtAu nanoparticles. Size distributions are each estimated from five images with the magnification of 100,000×.

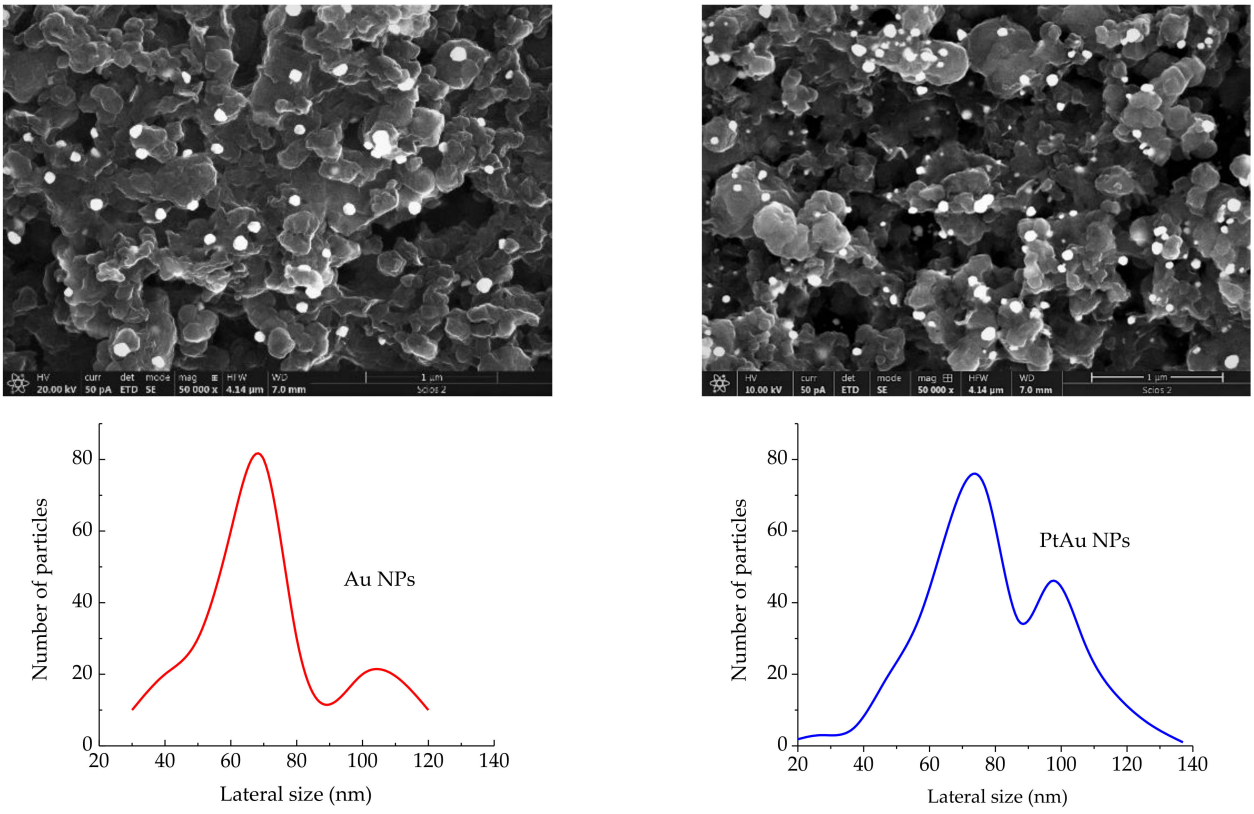

(**a**) (**b**)

Figure 1. SEM images (magnification = 50,000×, scale-bar = 1 µm) of: (**a**) Au/rGO and Au NPs size distribution; (**b**) PtAu/rGO and PtAu NPs size distribution.

The SEM image of Au/rGO, Figure 1a, shows a random distribution of the deposited Au nanoparticles over the graphene layer and their lateral size distribution. The size of Au nanoparticles is within the range of 30 to 120 nm. The deposited Au nanoparticles are almost uniform. According to the higher peak on the distribution curve, their average size is about 68 ± 10 nm. The second peak in the size distribution curve with a maximum at about 100 nm indicates the presence of agglomerated Au nanoparticles.

Figure 1b shows the SEM image of PtAu/rGO and the corresponding lateral size distribution of the deposited PtAu nanoparticles. After Pt deposition on previously prepared Au/rGO, the size distribution curve shows that the resulting PtAu nanoparticles are not uniform in size ranging from 20 to 140 nm. The average size of PtAu nanoparticles is about 73 ± 10 nm and falls within the higher peak in the size distribution curve. A smaller peak at about 110 nm indicates a smaller number of agglomerated particles. This

non-uniformity of PtAu nanoparticles size means that platinum is deposited partly on the previously deposited Au nanoparticles and partly on bare graphene edges.

The chemical composition analysis by energy dispersive X-ray spectroscopy (EDS), Figure 2, confirms that Au/rGO consists of carbon, oxygen, and gold, while PtAu/rGO consists of carbon, oxygen, gold, and platinum. Table 1 gives the weights and atomic percentages of these elements estimated as average values from the whole area over the presented SEM images. The estimated Au:Pt ratio of 2:1 for PtAu/rGO is only the average one. This ratio differs for the individual PtAu nanoparticles, all of which consist of gold and platinum.

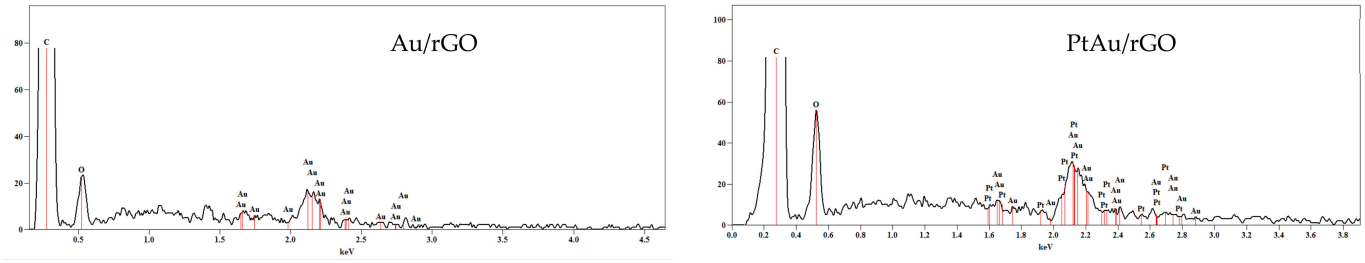

(**a**) (**b**)

Figure 2. EDS of: (**a**) Au/rGO; (**b**) PtAu/rGO.

Table 1. Weight and atomic percentages of C, O, Au and Pt in Au/rGO and PtAu/rGO obtained by EDS.

Element/Line Type	Au/rGO		PtAu/rGO	
	Weight %	Atom %	Weight %	Atom %
C K	85.63	94.76	81.32	93.80
O K	5.60	4.65	6.14	5.31
Au M	8.77	0.59	4.14	0.29
Pt M			8.40	0.60

2.1.2. XPS Characterization

The chemical composition of Au/rGO and PtAu/rGO was determined using X-ray photoelectron spectroscopy after subsequent Au and Pt deposition and additional potential cycling. In survey spectra of Au/rGO and PtAu/rGO, Figure 3, the main photoelectron lines C 1s, O 1s, and Au 4f, are denoted for both, but Pt 4f only for PtAu/rGO. These lines confirm the presence of C, O, Au, and Pt and no other elements or impurities. The intensities of C 1s and O 1s lines do not differ significantly for Au/rGO and PtAu/rGO due to the small amount of both deposits. The intensities of Au 4f doublet lines for Au/rGO do not significantly decrease after Pt deposition, meaning that Pt is deposited preferably on edges and less on top of already deposited Au. The oxidation state of Au and Pt and different functional groups in graphene support are determined by recording high-resolution spectra for all PtAu/rGO components.

Figure 4 shows high-resolution XPS spectra of C 1s, O 1s, Au 4f, and Pt 4f lines for the PtAu/rGO sample. The deconvolution of the C1s line, Figure 4a, gives five components for different carbon functional groups. A sharp C 1s component at the lowest binding energy at 284.9 eV corresponds to sp^2 carbon with C=C bonds and another at 285.1 eV to sp^3 carbon atoms in C–C bonds [26,27]. The other two components with higher binding energies at 286.6 eV and 286.9 eV correspond to sp^3 carbon atoms in the C–O bond in hydroxyl and the O–C=O carboxylate functional group, respectively [26–28]. The low-intensity wide peak at around 291.4 eV corresponds to a π–π^* satellite bond [28]. The relatively small intensity of oxygen-containing functional groups in the C 1s line indicates that the supporting graphene is reduced graphene oxide.

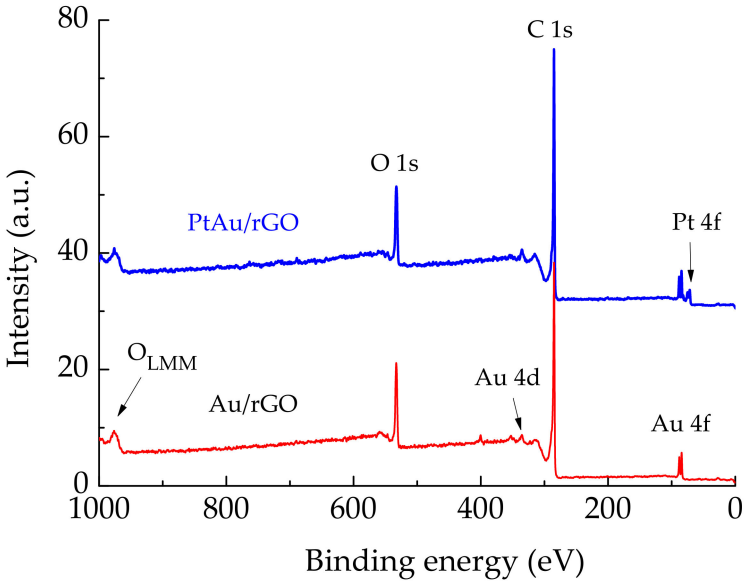

Figure 3. Survey spectra for rGO supported Au and PtAu nanoparticles.

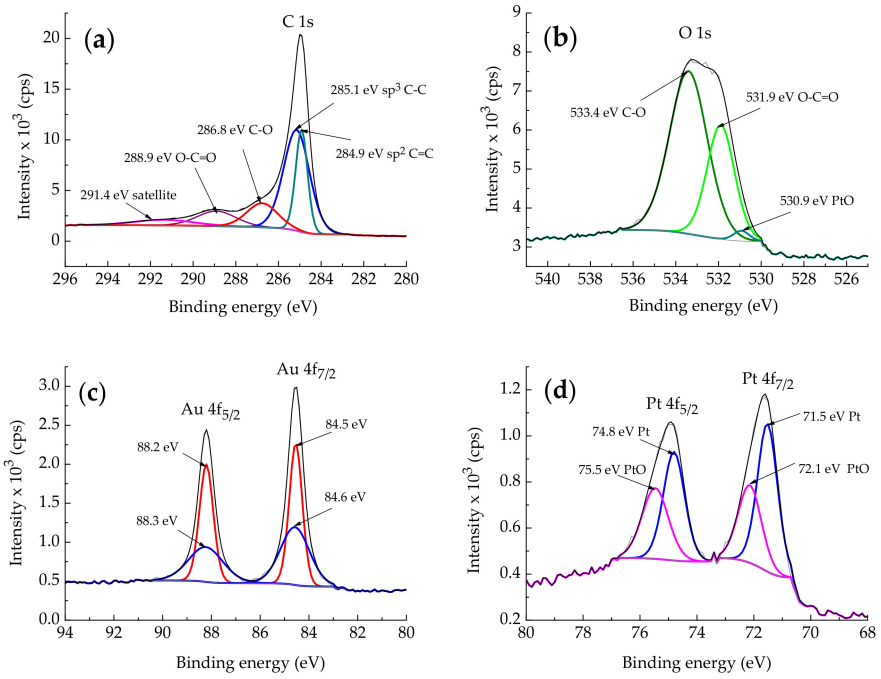

Figure 4. High-resolution XPS spectra for PtAu/rGO constituents showing the following deconvoluted peaks: (**a**) C 1s; (**b**) O 1s; (**c**) Au 4f; and (**d**) Pt 4f.

O 1s line, Figure 4b, is deconvoluted into three components with the peaks at 530.9 eV, 531.9 eV, and 533.4 eV. These peaks correspond to oxygen originating from Pt hydroxide from the deposited Pt nanoparticles [29], O–C=O, and C–O, respectively [28]. Oxygen peaks confirm the presence of oxygen-containing functional groups and indicate the presence of PtO in the deposited PtAu nanoparticles, as shown below.

Figure 4c shows Au 4f lines, each deconvoluted into two components. The higher intensity peaks at 84.5 eV and 88.2 eV, attributed to the bulk components of Au $4f_{7/2}$ and Au $4f_{5/2}$ lines, show a slight upward shift compared to bare metallic Au(111) [30,31] but agree with those for Au/rGO [21], such as the peaks at 84.6 eV and 88.3 eV of the corresponding surface components. Therefore, the shift of all Au 4f components can be attributed to the influence of graphene substrate and deposited Pt.

Figure 4d shows Pt 4f lines, each deconvoluted into two components. Components at 71.5 eV and 74.8 eV for Pt $4f_{7/2}$ and Pt $4f_{5/2}$, are from metallic Pt, while those at 72.1 eV and 75.5 eV are from PtO [30,32,33]. Pt 4f peaks are shifted from peaks for bare metallic Pt (71.1 eV and 74.4 eV for Pt $4f_{7/2}$ and Pt $4f_{5/2}$, respectively [30,32]) due to the lower coverage of the substrate surface with Pt nanoparticles and their interaction with the underlying substrate (in this case either graphene support or Au nanoparticles). Both O 1s components at 530.9 eV and for Pt $4f_{7/2}$ and Pt $4f_{5/2}$ components at 72.1 eV and 75.9 eV, respectively, confirm that Pt is oxidized partially to PtO, whose binding energies depend on the degree of bulk Pt oxidation [30], and in the case of supported Pt nanoparticles on the platinum coverage [32,33].

Table 2 shows the share in atomic percentages (atom %) of carbon, oxygen, gold, and platinum in Au/rGO and PtAu/rGO obtained from high-resolution XPS spectra. Due to the difference in graphene synthesis (see below Materials and Methods), the share of C 1s is slightly higher, and of O 1s lower than in the case reported in our previous work [21] for PdAu/rGO. The percentages of the deposited Au and Pt differ from Au and Pd for the same deposition conditions [21] due to a difference in supporting rGO. Besides, the intrinsic properties of the deposited Pt and Pd take a role in their deposition affinity.

Table 2. The share of carbon, oxygen, gold, and platinum in Au/rGO and PtAu/rGO.

Line	Au/rGO Atom %	PtAu/rGO Atom %
C 1s	83.3	82.8
O 1s	16.0	15.0
Au $4f_{7/2}$	0.7	0.6
Pt $4f_{7/2}$		0.3

2.2. Hydrogen Evolution on Au/rGO and PtAu/rGO

2.2.1. Cyclic Voltammetry Characterization of Au/rGO and PtAu/rGO

The cyclic voltammograms of rGO, Au/rGO, and PtAu/rGO electrodes recorded in 0.5 M H_2SO_4 with the same lower potential limit set at 0.01 V, are presented in Figure 5. The electrochemical characterization involved recording CVs in a positive potential window to observe the double-layer capacity of the electrodes, and a possible appearance of oxidation/reduction peaks of Au for Au/rGO, and hydrogen adsorption/desorption on platinum for PtAu/rGO electrode taking into account a small amount of both Au and Pt. CV curve of rGO in the potential range from 0.01 V to 0.71 V shows a characteristic shape comparable to our previous work [21]. A higher limit was set at a potential of 0.71 V to avoid further oxidation of graphene since hydrogen evolution measurements followed CV characterization. CV for Au/rGO electrode was recorded from 0.01 V to 1.66 V, with the higher limit set at a potential positive enough to identify Au oxidation/reduction. In the forward scan, Au oxidation begins at approx. 1.25 V, and proceeds with a higher current density at higher potentials, most likely due to the simultaneous oxygen evolution. In the reverse scan, a small AuO reduction peak appears at 1.17 V, confirming the presence of Au on Au/rGO [21,23,25].

CV for PtAu/rGO electrode was recorded from 0.01 V to 1.21 V, with previous conditioning by holding the potential at 0.11 V for 10 min to reduce the Pt oxide that originates from the deposition. The higher potential limit of 1.21 V was chosen low enough to avoid Pt oxidation and possible dissolution. Hydrogen evolution is already visible at lower potentials, and an anodic peak at 0.03 V, most likely originating from hydrogen oxidation on Pt [34], confirms successful Pt deposition. It is hard to distinguish hydrogen adsorption/desorption from hydrogen evolution/oxidation for such a small amount of the deposited platinum.

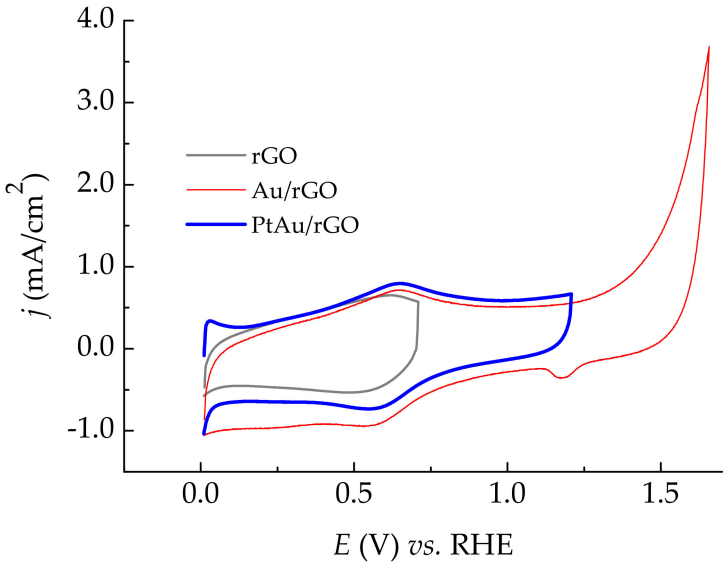

Figure 5. Cyclic voltammograms of rGO, Au/rGO, and PtAu/rGO. The scan rate was 50 mV/s.

2.2.2. HER Catalytic Activity of rGO, Au/rGO, and PtAu/rGO

The examination of the catalytic activity of the electrodes for HER involved LSV measurements in deaerated 0.5 M H_2SO_4, and the evaluation of the corresponding Tafel slopes, as illustrated in Figure 6. Hydrogen evolution reaction on Au/rGO, and PtAu/rGO was investigated in separate measurements, where spontaneous deposition of Au and Pt was followed by short conditioning at the initial potential, without any previous potential cycling.

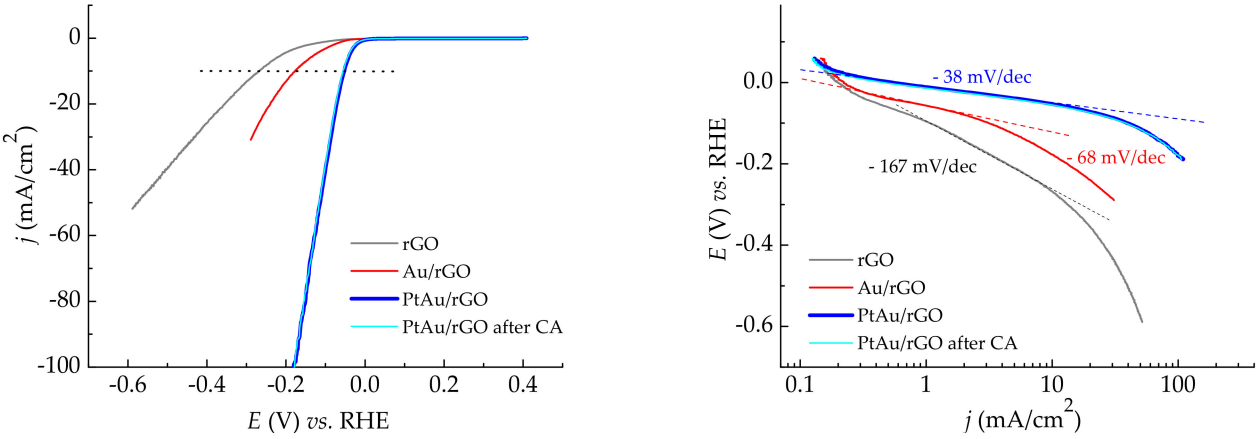

Figure 6. Hydrogen evolution reaction in 0.5 M H_2SO_4: (**a**) LSV curves recorded at a scan rate of 10 mV/s for rGO, Au/rGO, and PtAu/rGO electrodes, as well as for PtAu/rGO alone after stability test; (**b**) Derived Tafel slopes.

LSV curves, Figure 6a, show a significant shift of the HER onset potentials starting from rGO, with the subsequent addition of small amounts of Au and Pt. The onset potential on LSV curves is where the current density increases visibly from zero. That means that the tangent line, drawn to estimate the onset potentials, is not at zero, due to the overlap of the current densities corresponding to the double-layer and HER. Setting up the tangent lines after subtracting the corresponding contribution of the double-layer current densities (see CVs in Figure 5), the obtained onset potential values are −0.1 V for rGO, −0.05 V for Au/rGO, and −0.005 V for PtAu/rGO. At a higher current density of −10 mA/cm^2 (denoted by a dotted line in Figure 6a), the obtained potentials for HER are −0.27 mV for

rGO, −0.18 mV for Au/rGO, and −0.05 V for PtAu/rGO. The rGO and Au/rGO electrodes are more active for HER than previously reported for PdAu/rGO system [21], while the addition of only a small amount of Pt on Au/rGO decreases the overpotential for HER for 130 mV. PtAu/rGO electrode alone has extraordinarily high activity, which remains approximately equal after stability measurements.

Figure 6b shows derived Tafel slopes. The slope of −167 mV/dec for rGO confirms its low activity as already reported [35]. For Au/rGO, the slope of −68 mV/dec differs from previously reported for a similar Au/rGO electrode [21], although the reaction occurs with a relatively higher rate, but also following a Volmer-Heyrovsky pathway [36,37]. The lowest Tafel slope of −38 mV/dec obtained for HER on PtAu/rGO indicates a much faster reaction rate, meaning that the electrode activity approaches the activity of bare Pt [1,22]. Supposedly, hydrogen evolution on PtAu/rGO also proceeds according to Volmer-Heyrovsky reaction pathway. It is worth noting that the reaction mechanism, including a rate-determining step, cannot be determined with certainty owing to its dependence on the potential that reflects on the coverage of adsorbed hydrogen [38].

2.2.3. EIS Measurements

Figure 7 shows the results obtained using the electrochemical impedance spectroscopy method to examine HER kinetics on PtAu/rGO electrode. Figure 7a shows the Nyquist plots for rGO and PtAu/rGO electrodes at a potential of −0.06 V vs. RHE.

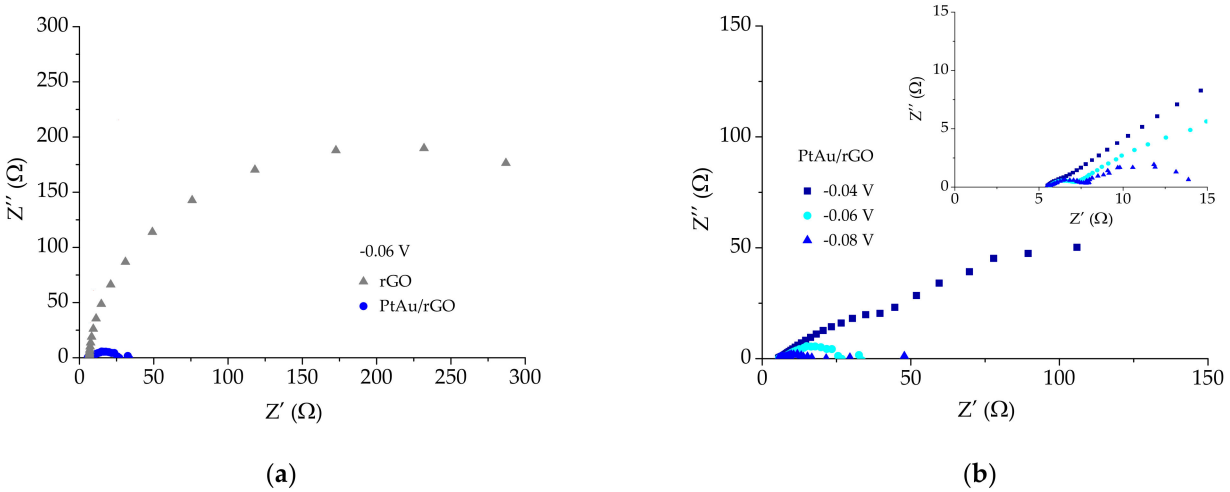

Figure 7. Nyquist plots for HER on PtAu/rGO electrode in 0.5 M H_2SO_4 for: (**a**) rGO and PtAu/rGO electrodes; (**b**) PtAu/rGO electrode at several applied potentials. Inset shows the details at a high frequency region.

The PtAu/rGO electrode shows a smaller semicircle, meaning the faster electron transfer rate and higher HER kinetics when compared to the substrate rGO electrode. This is in agreement with LSV results. Furthermore, the PtAu/rGO electrode was examined at electrode potentials of −0.04, −0.06, and −0.08 V vs. RHE, and Nyquist plots are presented in Figure 7b.

The interpretation of these impedance data involved the construction of the Armstrong and Henderson equivalent electric circuit [39–42]. Figure 8 shows the electric circuit, where R_s is the solution resistance, R1 is the charge transfer resistance related to the reaction at the working electrode, and CPE1 to the double-layer capacitance. R2 is the pseudo-resistance concerning mass transfer resistance of the adsorbed hydrogen intermediate. CPE2 is a working electrode pseudo-capacitance.

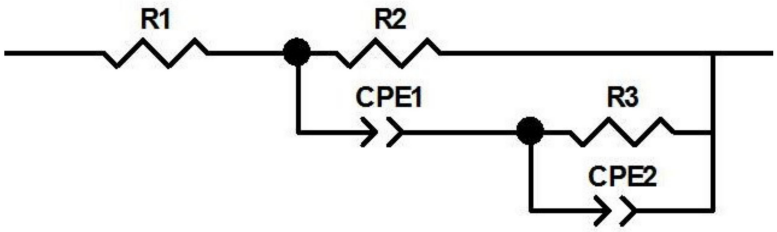

Figure 8. The equivalent electric circuit, used for fitting the data.

Table 3 shows the parameters obtained by fitting the EIS data. The values obtained for R_s have a slightly increasing trend with a decrease in the applied potential in line with the increasing number of bubbles in the electrolyte [40]. The charge transfer resistance, R1, and the pseudo-resistance, R2, show a decreasing trend with increasing applied electrode potentials. These results suggest the improved electron-transfer kinetics with increasing electrode potentials [43], as indicated by the increasing current density in LSV curves.

Table 3. The parameters, obtained from EIS data for PtAu/rGO at different applied potentials.

E (V) vs. RHE	−0.04	−0.06	−0.08
Rs (Ω)	5.33	5.55	5.78
R2 (Ω)	11.8	2.28	2.4
R3 (Ω)	262.6	20.8	11.8
CPE1 (F)	27.8×10^{-3}	4.98×10^{-3}	1.958×10^{-3}
CPE2 (F)	3.075×10^{-3}	72.04×10^{-3}	0.127

2.2.4. Stability Test for Hydrogen Evolution on PtAu/rGO

Chronoamperometry was used to test the stability and durability of the most active PtAu/rGO electrode. It was performed in deaerated 0.5 M H_2SO_4 with a rotating disc electrode at a rotation rate of 2500 rpm. Chronoamperometry (CA) curve, Figure 9, is recorded at a constant potential of −0.02 V held for 40 min. The high current density of −3.7 mA/cm^2 was reached almost immediately and only slightly decreased during the measurement time. The LSV curve recorded after CA measurements showed the identical electrode activity as before the stability test, demonstrating the PtAu/rGO electrode stability for a prolonged time.

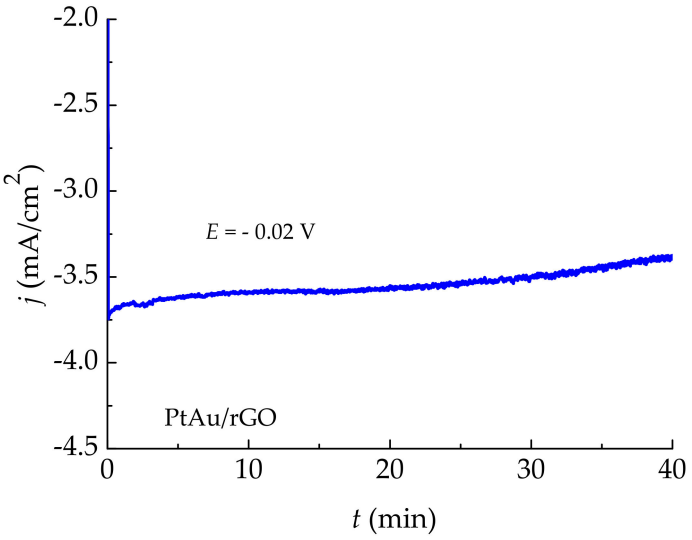

Figure 9. Chronoamperometry curve for PtAu/rGO recorded in 0.5 M H_2SO_4 at a constant potential of −0.02 V.

The activity parameters for HER on previously studied PtAu catalysts supported on carbon-based materials in 0.5 M H_2SO_4 solution, involving the onset potentials and Tafel slopes, are listed in Table 4.

Table 4. Comparison of the activity of various PtAu catalysts for HER in 0.5 M H_2SO_4 solution.

Catalyst	Onset Potential *E* (mV) vs. RHE	Tafel Slope (mV/dec)	Ref.
Au@Pt NPs/rGO	−20	42	[22]
Au-monolayer Pt/rGO	≈0	27	[23]
AuPt@Pt nanocrystals/rGO	−25	33	[24]
AuPt alloy nanodendrites/rGO	−37	34	[25]
Au-Pt (54:47) alloy NPs/GC	−6	34	[44]
$Au_{38·4}$@$Au_{9·3}Pt_{52·3}$ -NP/C	−4	14	[45]
Pt/C	−5	31	[45]
PtAu/rGO	−5	38	This work

In this wok the onset potential for HER on PtAu/rGO is similar or better than most PtAu catalysts supported by rGO or the other carbon-based materials listed in Table 4, including the best performance of a commercial Pt/C catalyst found in the literature.

3. Materials and Methods

3.1. Materials Preparation

The synthesis of graphene powder involved the electrochemical exfoliation of spectral graphite (carbon rod, 5 mm diameter, Specpure, Grade 2, Johnson Matthey Chemicals Ltd., London, UK) as described in detail in ref. [21]. Instead of drying graphene powder at a higher temperature, in this case, the drying at room temperature was performed. As a result, the obtained rGO contained a bit lower at% of carbon and higher of oxygen. GC disc (7 mm diameter, geometric area 0.385 cm^2.) was as a supporting electrode for SEM and XPS measurements, and GC disc (5 mm diameter, geometric area 0.196 cm^2), embedded in a Teflon holder for the electrochemical measurements. The supporting rGO/GC electrode was prepared by spreading three drops of 3 g/L of graphene powder suspension on GC support in the total quantity of 15 µL (0.045 mg rGO) on 5 mm diameter GC, and 6 drops containing the total quantity of 30 µL (0.090 mg rGO) on 7 mm in diameter GC. Such a supporting electrode was immersed for 10 min in a 1 mM $HAuCl_4$ + 0.5 M H_2SO_4 solution to allow the gold to deposit spontaneously at the open circuit potential. After rinsing with water, a working Au/rGO electrode was prepared. Finally, the PtAu/rGO electrode was obtained by subsequent immersion of previously prepared Au/rGO for 30 min spontaneous deposition at the OCP of platinum from 1 mM H_2PtCl_4 + 0.5 M H_2SO_4 solution. After a final rinsing with water, the electrodes were dried and characterized by XPS and SEM.

3.2. Materials Characterization

SEM images and EDS spectra were recorded using FESEM (FEI Scios 2) (Thermo Fisher Scientific, Waltham, MA, USA) at the pressure of 1×10^{-4} Pa with the electron beam voltage of 10 kV. The time for spectrum acquisition from the chosen micro areas was 30 min.

XPS spectra were acquired by SPECS Systems using an XP50M X-ray source (SPECS Surface Nano Analysis GmbH, Berlin, Germany) with AlKα source (1486.74 eV) at 12.5 kV and 32 mA. The chamber pressure was 9×10^{-9} mbar. Survey spectra (0–1000 eV binding energy) of Au/rGO and PtAu/rGO were aquired using a constant pass energy of 40 eV, step size 0.5 eV, and dwell time 0.2 s. For PtAu/rGO, high-resolution spectra were collected for C 1s, O 1s, Au 4f, and Pt 4f photoelectron lines using a constant pass energy of 20 eV, step size 0.1 eV, and dwell time 2 s. The sample charging was neutralized by SPECS FG15/40 flood gun. All peak positions are given relative to C 1s at 284.8 eV.

3.3. Electrochemical Measurements

Electrochemical measurements were conducted by Gamry potentiostat PCl4 (Warminster, PA, USA) in a three-electrode cell, with Pt wire as counter and Ag/AgCl, 3 M KCl as a reference electrode.The working electrodes mounted in a Teflon holder were rGO, Au/rGO, or PtAu/rGO. All potential scales and values were given vs. the reference hydrogen electrode (RHE). The obtained electrodes were characterized, and their HER activity was examined by cyclic and linear sweep voltammetry in a deaerated 0.5 M H_2SO_4 solution. Electrochemical impedance spectroscopy measurements were performed in the same solution at different applied potentials. The amplitude was 5 mV, and the frequency ranged from 20 kHz to 0.01 Hz.

3.4. Chemicals

The solutions were prepared using supra pure H_2SO_4 (Merck, Darmstadt, Germany), $HAuCl_4$(aq) (MaTeck, Jülich, Germany), H_2PtCl_4 (Alfa Aesar, Thermo Fisher Scientific, Kandel, Germany), and Milli-pure water. All solutions were deaerated by N_2 (99.9995%, Messer, Frankfurt, Germany).

4. Conclusions

In this work, we demonstrate the remarkable catalytic activity of PtAu/rGO for hydrogen evolution in sulfuric acid solution. SEM images show that randomly distributed and non-uniform in size PtAu nanoparticles are situated primarily on the edges of rGO sheets. EDS and XPS analysis both confirm the low atomic percentage of gold (0.6 at%) and platinum (0.3 at%). The LSV curve for the PtAu/rGO electrode shows the outstanding onset potential for HER of −0.005 V and a low Tafel slope of −38 mV/dec. EIS analyses agree with LSV results, indicating high HER activity. The CA measurement performed for 40 min at a constant electrode potential shows good stability and durability of the PtAu/rGO catalyst for hydrogen evolution.

Author Contributions: Conceptualization, L.R., S.Š. and I.S.; graphene synthesis, A.M.; SEM characterization, V.R., L.R. and I.S.; XPS characterization, L.R., CV and LSV electrochemical measurements, L.R.; EIS measurements I.S.S.; writing—original draft preparation, L.R., I.S.S. and I.S.; writing—review and editing, S.Š.; supervision, I.S. All authors have read and agreed to the published version of the manuscript.

Funding: This research was funded by the Ministry of Education, Science and Technological Development of the Republic of Serbia.

Conflicts of Interest: The authors declare no conflict of interest.

References

1. Shinagawa, T.; Takanabe, K. Towards versatile and sustainable hydrogen production through electrocatalytic water splitting: Electrolyte engineering. *ChemSusChem* **2017**, *10*, 1318–1336. [CrossRef]
2. Dincer, I. Green methods for hydrogen production. *Int. J. Hydrog. Energy* **2012**, *37*, 1954–1971. [CrossRef]
3. Thomas, J.M.; Edwards, P.P.; Dobson, P.J.; Owen, G.P. Decarbonising energy: The developing international activity in hydrogen technologies and fuel cells. *J. Energy Chem.* **2020**, *51*, 405–415. [CrossRef]
4. Bhalothia, D.; Krishnia, L.; Yang, S.-S.; Yan, C.; Hsiung, W.-H.; Wang, K.-W.; Chen, T.-Y. Recent advancements and future prospects of noble metal-based heterogeneous nanocatalysts for oxygen reduction and hydrogen evolution reactions. *Appl. Sci.* **2020**, *10*, 7708. [CrossRef]
5. Li, C.; Baek, J.-B. Recent advances in noble metal (Pt, Ru, and Ir)-based electrocatalysts for efficient hydrogen evolution reaction. *ACS Omega* **2020**, *5*, 31–40. [CrossRef] [PubMed]
6. Eftekhari, A. Electrocatalysts for hydrogen evolution reaction. *Int. J. Hydrog. Energy* **2017**, *42*, 11053–11077. [CrossRef]
7. Pu, Z.; Amiinu, I.S.; Cheng, R.; Wang, P.; Zhang, C.; Mu, S.; Zhao, W.; Su, F.; Zhang, G.; Liao, S.; et al. Single-Atom Catalysts for Electrochemical Hydrogen Evolution Reaction: Recent Advances and Future Perspectives. *Nano-Micro Lett.* **2020**, *12*, 21. [CrossRef]
8. Liu, H.; Xianyun Peng, X.; Liu, X. Single-Atom Catalysts for the Hydrogen Evolution Reaction. *ChemElectroChem* **2018**, *5*, 2963–2974. [CrossRef]

9. Cheng, N.; Stambula, S.; Wang, D.; Banis, M.N.; Liu, J.; Riese, A.; Xiao, B.; Li, R.; Sham, T.-K.; Liu, L.-M.; et al. Platinum single-atom and cluster catalysis of the hydrogen evolution reaction. *Nat. Commun.* **2016**, *7*, 13638. [CrossRef]
10. Tian, Y.; Yu, L.; Zhuang, C.; Zhang, G.; Sun, S. Fast synthesis of Pt single-atom catalyst with high intrinsic activity for hydrogen evolution reaction by plasma sputtering. *Mater. Today Energy* **2021**, *22*, 100877. [CrossRef]
11. Li, J.; Banis, M.N.; Ren, Z.; Adair, K.R.; Doyle-Davis, K.; Meira, D.M.; Finfrock, Y.Z.; Zhang, L.; Kong, F.; Sham, T.-K.; et al. Unveiling the Nature of Pt Single-Atom Catalyst during Electrocatalytic Hydrogen Evolution and Oxygen Reduction Reactions. *Small* **2021**, *17*, 2007245. [CrossRef]
12. Wang, D.; Li, Q.; Han, C.; Xing, Z.; Yang, X. Single-atom ruthenium based catalyst for enhanced hydrogen evolution. *Appl. Catal. B Environ.* **2019**, *249*, 91–97. [CrossRef]
13. Hossain, M.D.; Liu, Z.; Zhuang, M.; Yan, X.; Xu, G.L.; Gadre, C.A.; Tyagi, A.; Abidi, I.H.; Sun, C.-J.; Wong, H.; et al. Rational design of graphene-supported single atom catalysts for hydrogen evolution reaction. *Adv. Energy Maert.* **2019**, *9*, 1803689. [CrossRef]
14. Ding, S.; Lyu, Z.; Zhong, H.; Liu, D.; Sarnello, E.; Fang, L.; Xu, M.; Engelhard, M.H.; Tian, H.; Li, T.; et al. An Ion-Imprinting Derived Strategy to Synthesize Single-Atom Iron Electrocatalysts for Oxygen Reduction. *Small* **2021**, *17*, 2004454. [CrossRef]
15. Jing, H.; Zhu, P.; Zheng, X.; Zhang, Z.; Wang, D.; Li, Y. Theory-oriented screening and discovery of advanced energy transformation materials in electrocatalysis. *Ceram. Int.* **2021**, *in press*. [CrossRef]
16. Murthya, A.P.; Madhavana, J.; Murugan, K. Recent advances in hydrogen evolution reaction catalysts on carbon/carbon-based supports in acid media. *J. Power Sources* **2018**, *398*, 9–26. [CrossRef]
17. Novoselov, K.S.; Geim, A.K.; Morozov, S.V.; Jiang, D.; Zhang, Y.; Dubonos, S.V.; Grigorieva, I.V.; Firsov, A.A. Electric field effect in atomically thin carbon films. *Science* **2004**, *306*, 666–669. [CrossRef] [PubMed]
18. Nemiwal, M.; Zhang, T.C.; Kumar, D. Graphene-based electrocatalysts: Hydrogen evolution reactions and overall water splitting. *Int. J. Hydrog. Energy* **2021**, *46*, 21401–21418. [CrossRef]
19. Huang, H.; Yan, M.; Yang, C.; He, H.; Jiang, Q.; Yang, L.; Lu, Z.; Sun, Z.; Xu, X.; Bando, Y.; et al. Graphene nanoarchitectonics: Recent advances in graphene-based electrocatalysts for hydrogen evolution reaction. *Adv. Mater.* **2019**, *31*, 1903415. [CrossRef] [PubMed]
20. Huang, C.; Li, C.; Shi, G. Graphene based catalysts. *Energy Environ. Sci.* **2012**, *5*, 8848–8868. [CrossRef]
21. Rakočević, L.; Srejić, I.; Maksić, A.; Golubović, J.; Štrbac, S. Hydrogen evolution on reduced graphene oxide-supported PdAu nanoparticles. *Catalysts* **2021**, *11*, 481. [CrossRef]
22. Shi, Y.-C.; Chen, S.-S.; Feng, J.-J.; Lin, X.-X.; Wang, W.; Wang, A.J. Dicationic ionic liquid mediated fabrication of Au@Pt nanoparticles supported on reduced graphene oxide with highly catalytic activity for oxygen reduction and hydrogen evolution. *Appl. Surf. Sci.* **2018**, *441*, 438–447. [CrossRef]
23. Shi, Y.; Zhai, T.T.; Zhou, Y.; Xu, W.-X.; Yang, D.-R.; Wang, F.-B.; Xia, X.-H. Atomic level tailoring of the electrocatalytic activity of Au-Pt core-shell nanoparticles with controllable Pt layers toward hydrogen evolution reaction. *J. Electroanal. Chem.* **2018**, *819*, 442–446. [CrossRef]
24. Shao, F.-Q.; Lin, X.-X.; Feng, J.-J.; Yuan, J.; Chen, J.-R.; Wang, A.-J. Simple fabrication of core-shell AuPt@Pt nanocrystals supported on reduced graphene oxide for ethylene glycol oxidation and hydrogen evolution reactions. *Electrochim. Acta* **2016**, *219*, 321–329. [CrossRef]
25. Feng, J.-J.; Chen, L.-X.; Ma, X.; Yuan, J.; Chen, J.-R.; Wang, A.-J.; Xu, Q.-Q. Bimetallic AuPt alloy nanodendrites/reduced graphene oxide: One-pot ionic liquid-assisted synthesis and excellent electrocatalysis towards hydrogen evolution and methanol oxidation reactions. *Int. J. Hydrog. Energy* **2017**, *42*, 1120–1129. [CrossRef]
26. Liu, C.-Y.; Lai, C.-H.; Lin, C.-C.; Yang, C.-P. Insertion of a graphene oxide layer into a $Cu/SiO_2/Pt$ structure to overcome performance degradation in a vaporless environment. *Appl. Sci.* **2019**, *9*, 1432. [CrossRef]
27. Eng, A.Y.S.; Sofer, Z.; Sedmidubský, D.; Pumera, M. Synthesis of Carboxylated-graphenes by the Kolbe-Schmitt process. *ACS Nano* **2017**, *11*, 1789–1797. [CrossRef] [PubMed]
28. Al-Gaashani, R.; Najjar, A.; Zakaria, Y.; Mansour, S.; Atieh, M.A. XPS and structural studies of high quality graphene oxide and reduced graphene oxide prepared by different chemical oxidation methods. *Ceram. Int.* **2019**, *45*, 14439–14448. [CrossRef]
29. Peuckert, M.; Coenen, F.P.; Bonzel, H.P. XPS study of the electrochemical surface oxidation of Platinum in N H_2SO_4 acid electrolyte. *Electrochim. Acta* **1984**, *29*, 1305–1314. [CrossRef]
30. Heimann, P.; Van der Veen, J.F.; Eastman, D.E. Structure-dependent surface core level shifts for the Au(111), Au(100), and Au(110) surfaces. *Solid State Commun.* **1981**, *38*, 595–598. [CrossRef]
31. Štrbac, S.; Smiljanić, M.; Rakočević, Z. Spontaneously deposited Rh on Au(111) observed by AFM and XPS: Electrocatalysis of hydrogen evolution. *J. Electrochem. Soc.* **2016**, *163*, D3027–D3033. [CrossRef]
32. Romeo, M.; Majerus, J.; Legare, P.; Castellani, N.; Leroy, D. Photoemission study of Pt adlayers on Ni(111). *Surf. Sci.* **1990**, *238*, 163–168. [CrossRef]
33. Zhang, J.-J.; Wang, Z.-B.; Li, C.; Zhao, L.; Liu, J.; Zhang, L.-M.; Gu, D.-M. Multiwall-carbon nanotube modified by N-doped carbon quantum dots as Pt catalyst support for methanol electrooxidation. *J. Power Sources* **2015**, *289*, 63–70. [CrossRef]
34. Zhang, Y.; Shao, Z.; Shen, Q.; Li, M.; Xu, L.; Luo, Z. Aqueous Preparation of platinum nanoflowers on three-dimensional graphene for efficient methanol oxidation. *Catalysts* **2018**, *8*, 519. [CrossRef]
35. Ferrari, A.G.M.; Brownson, D.A.C.; Banks, C.E. Investigating the integrity of graphene towards the electrochemical hydrogen evolution reaction (HER). *Sci. Rep.* **2019**, *9*, 15961. [CrossRef] [PubMed]

36. Smiljanić, M.; Srejić, I.; Grgur, B.; Rakočević, Z.; Štrbac, S. Catalysis of hydrogen evolution on Au(111) modified by spontaneously deposited Pd islands. *Electrocatalysis* **2012**, *3*, 369–375. [CrossRef]
37. Wang, Y.; Sun, Y.; Liao, H.; Sun, S.; Li, S.; Ager, J.W., III; Xu, Z.J. Activation effect of electrochemical cycling on gold nanoparticles towards the hydrogen evolution reaction in sulfuric acid. *Electrochim. Acta* **2016**, *209*, 440–447. [CrossRef]
38. Shinagava, T.; Garcia-Espanza, A.T.; Takanabe, K. Insight on Tafel slopes from a microkinetic analysis of aqueous electrocatalysis for energy conversion. *Sci. Rep.* **2015**, *5*, 13801. [CrossRef]
39. Armstrong, R.D.; Henderson, M. Impedance plane display of a reaction with an adsorbed intermediate. *J. Electroanal. Chem.* **1972**, *39*, 81–90. [CrossRef]
40. Amaral, L.; Cardoso, D.S.P.; Šljukić, B.; Santos, D.M.F.; Sequeira, C.A.C. Electrochemistry of hydrogen evolution in ionic aqueous mixtures. *Mater. Res. Bull.* **2019**, *112*, 407–412. [CrossRef]
41. Franceschini, E.A.; Lacconi, G.I.; Corti, H.R. Kinetics of the hydrogen evolution on nickel in alkaline solution: New insight from rotating disk electrode and impedance spectroscopy analysis. *Electrochim. Acta* **2015**, *159*, 210–218. [CrossRef]
42. Krstajić, N.; Popović, M.; Grgur, B.; Vojnović, M.; Šepa, D. On the kinetics of the hydrogen evolution reaction on nickel in alkaline solution—Part I. The mechanism. *J. Electroanal. Chem.* **2001**, *512*, 16–26. [CrossRef]
43. Liu, Y.; Ren, L.; Zhang, Z.; Qi, H.; Li, H.; Zhong, J. 3D binder-free $MoSe_2$ nanosheets/carbon cloth electrodes for efficient and stable hydrogen evolution prepared by simple electrophoresis deposition strategy. *Sci. Rep.* **2016**, *6*, 22516. [CrossRef]
44. Mirdamadi-Esfahani, M.; Mostafavi, M.; Keita, B.; Nadjo, L.; Kooyman, P.; Remita, H. Bimetallic Au-Pt nanoparticles synthesized by radiolysis: Application in electro-catalysis. *Gold Bull.* **2010**, *43*, 49–56. [CrossRef]
45. Cao, Y.; Xiahou, Y.; Xing, L.; Zhang, X.; Li, H.; Wu, C.S.; Xia, H. Fe(II)-assisted one-pot synthesis of ultra-small core-shell Au-Pt nanoparticles as superior catalysts towards HER and ORR. *Nanoscale* **2020**, *12*, 20456–20466. [CrossRef]